Effects of Calcium Carbonate and Its Purity on Crystallization and Melting Behavior, Mechanical Properties, and Processability of Syndiotactic Polypropylene

3 AUTHORS, INCLUDING:

Pitt Supaphol
Chulalongkorn University

234 PUBLICATIONS   **6,427** CITATIONS

Effects of Calcium Carbonate and Its Purity on Crystallization and Melting Behavior, Mechanical Properties, and Processability of Syndiotactic Polypropylene

Pitt Supaphol, Wipasiri Harnsiri, Jirawut Junkasem

The Petroleum and Petrochemical College, Chulalongkorn University, Soi Chula 12, Phyathai Road, Pathumwan, Bangkok 10330, Thailand

ABSTRACT: Calcium carbonate-filled syndiotactic poly-(propylene) ($CaCO_3$-filled s-PP) was prepared in a self-wiping, co-rotating twin-screw extruder. The effects of $CaCO_3$ of varying particle size (1.9, 2.8 and 10.5 μm), content (0–40 wt %), and type of surface modification (uncoated, stearic acid-coated, and paraffin-coated) on the crystallization and melting behavior, mechanical properties, and processability of $CaCO_3$-filled s-PP were investigated. Non-isothermal crystallization studies indicate that $CaCO_3$ acts as a good nucleating agent for s-PP. The nucleating efficiency of $CaCO_3$ for s-PP was found to depend strongly on its purity, type of surface treatment, and average particle size. Tensile strength was found to decrease, while Young's modulus increased, with increasing $CaCO_3$ content. Both types of surface treatment on $CaCO_3$ particles reduced tensile strength and Young's modulus, but improved impact resistance. Scanning electron microscopy (SEM) observations of the fracture surfaces for selected $CaCO_3$-filled s-PP samples revealed an improvement in $CaCO_3$ dispersion as a result of surface treatment. Finally, steady-state shear viscosity of $CaCO_3$-filled s-PP was found to increase with increasing $CaCO_3$ content and decreasing particle size. © 2004 Wiley Periodicals, Inc. J Appl Polym Sci 92: 201–212, 2004

Key words: syndiotactic; poly(propylene); crystallization; mechanical properties; processing

INTRODUCTION

In 1988, Ewen et al.[1] reported a successful synthesis of stereo-regular and regio-regular syndiotactic poly(propylene) (s-PP) via a novel metallocene catalysis, instead of the traditional Ziegler–Natta catalysis.[2] The discovery of this new catalyst system provided a new route for producing s-PP with improved purity and yield, which led to renewed interest for both scientific research[3] and industrial applications.[4–8]

Studies of the crystallization process of semicrystalline polymers are of great importance in polymer processing, because the resulting physical properties are strongly related to the morphology and the extent of crystallization. Both quiescent isothermal and non-isothermal crystallization studies revealed that s-PP is a slowly crystallizing polymer.[9,10] The addition of nucleating agents may help to overcome this problem by providing more nucleation sites, resulting in an increase in the overall crystallization rate, and hence reducing the processing time.

Nucleating agents can be divided into two types: inorganic and organic. Inorganic nucleating agents include talc, mica, barium sulfate ($BaSO_4$) and calcium carbonate ($CaCO_3$). Organic nucleating agents include sorbitals and their derivatives. Generally, $CaCO_3$ is added to isotactic poly(propylene) (i-PP) to reduce the cost of the product, improve mechanical properties (e.g. modulus and heat stability), and enhance crystallization rate. To our knowledge, the only available reports on filled systems in s-PP, conducted by Mülhaupt and co-workers,[11–13] are concerned with the mechanical and thermal properties, including phase behavior, of s-PP filled with glass beads and talcum.

In this study, the effects of $CaCO_3$ of varying particle size (1.9, 2.8 and 10.5 μm), content (0–40 wt %), and type of surface modification (uncoated, stearic acid-coated, and paraffin-coated) on the crystallization and melting behavior, mechanical properties (tensile and impact properties), and processability (steady-state shear viscosity) of s-PP/$CaCO_3$ compounds were studied and reported for the first time.

EXPERIMENTAL

Materials

A commercial grade s-PP was produced and supplied in pellet form by ATOFINA Petrochemicals, Inc. (Houston, Texas, USA). Molecular characterization for this resin was carried out by Dr. Roger A. Phillips of

---

TABLE I
Characteristics of CaCO$_3$ Grades Used

Trade Name	Average particle size (μm)	Type of surface treatment
CALOFIL 400	1.9	Uncoated
CALOFIL 100	2.8	Uncoated
CALOFIL 50	10.5	Uncoated
HICOAT 410	1.9	Stearic acid-coated
HICOAT P-400	1.9	Paraffin-coated

Basell USA, Inc. (Elkton, Maryland, USA). The results show the following molecular weight information: the weight-average molecular weight (M_w) = 153,000 Da and the polydispersity (M_w/M_n) = 3.8. Syndiotacticity of this resin was determined by ^{13}C-NMR to exhibit the racemic triad content (%rr) of 86.1% and the racemic pentad content (%$rrrr$) of 73.7%, with a very low ethylene defect content of less than 0.5 wt %.

Five commercial grades of CaCO$_3$, kindly supplied by Calcium Products Co.,Ltd. (Thailand), were used as received. Particle characteristics of all CaCO$_3$ grades (all with a density of $\approx$2.7 g/cm^3) used are listed in Table I. Characterization of all CaCO$_3$ grades by X-ray diffraction revealed that most of the as-received grades exhibited strong reflection peaks at 2θ = 29.0, 39.4 and 43.2°, corresponding to the characteristic peaks of calcite (JCPDS card no. 5-586), with the exception of the 10.5 μm uncoated CaCO$_3$ grade (CALOFIL 50), which exhibited strong reflection peaks, in addition to those of calcite, at 2θ = 30.9, 41.1 and 51.0°, corresponding to the peaks of calcium magnesium carbonate or dolomite [CaMg(CO$_3$)$_2$] (JCPDS card no. 36-426). This means that the as-received 10.5 μm uncoated CaCO$_3$ grade contained not only calcite but also dolomite.

Sample preparation

CaCO$_3$ with varying particle size and type of surface treatment (uncoated, stearic acid-coated, and paraffin-coated) was first dried in an oven at 80°C for 14 h and then pre-mixed with s-PP resin in a tumble mixer for 10 min in various compositional ratios, ranging from 0 to 40 wt % (approx. 0 to 18 vol %). The pre-mixed compounds were then melt-mixed in a Collin ZK 25 self-wiping, co-rotating twin-screw extruder operating at a screw speed of 50 rpm and a die temperature of 190°C. The extrudate was cooled in water and cut into pellet form by a Planetrol 075D2 pelletizer. A Wabash V50H compression press was used to prepare films and sheets of both neat s-PP and s-PP/CaCO$_3$ compounds for subsequent tests. The mold was first pre-heated in the compression press at 190°C for 5 min and then compressed with a 15 ton-force for another 5 min, after which it was cooled to 40°C.

Differential scanning calorimetry measurements

Non-isothermal crystallization behavior of CaCO$_3$-filled s-PP samples was investigated on a Perkin–Elmer Series 7 differential scanning calorimeter (DSC). Temperature calibration was performed using an indium standard (T_m^o = 156.6°C and ΔH_f^o = 28.5 J/g). Each sample of 3 to 6 mg in weight, cut from the prepared compressed films, was sealed in an aluminum sample holder. The experimental procedure started with melting each sample at 190°C for 5 min and then cooling it to −5°C at a rate of 10°C/min. After that, the sample was immediately subjected to heating at a rate of 20°C/min to 160°C. Both the crystallization exotherm and the melting endotherm were recorded for further analysis. All measurements were carried out in nitrogen atmosphere.

Crystal structure and crystallinity measurements

A wide-angle X-ray diffraction (WAXD) technique was used to determine the crystal modification and the apparent degree of crystallinity for both neat and CaCO$_3$-filled s-PP samples prepared according to the conditions set forth for DSC measurements but without a subsequent heating step. Each sample was removed from the DSC sample holder and pasted onto a glass sample holder. The WAXD intensity patterns of the sample were then collected on a Rigaku Rint2000 diffractometer (CuK$_\alpha$ radiation, λ = 1.54 Å), equipped with computerized data collection and analytical tools. The X-ray source was operated at a voltage of 40 kV and a filament current of 30 mA.

Mechanical property measurements

Tensile strength and modulus for both neat and CaCO$_3$-filled s-PP samples were measured on an Instron 4206 universal testing machine according to ASTM D 638-91 standard test method using a 100 kN load cell and a 50 mm/min crosshead speed. Izod impact resistance was determined on a Swick 5113 impact tester according to ASTM D 256-90b standard test method using 2.7 J pendulum and 124.4° release angle. The results are reported as averages of the data taken from at least five specimens.

Microstructural observation

A JEOL 520-2AE scanning electron microscope (SEM) was used to observe the microstructure of the impact-fractured surfaces of selected specimens obtained after impact testing. Each selected specimen was cut about 2 mm below the fractured surface, and the cut piece was stuck onto an aluminum stub. The sample was coated with gold using a vapor deposition technique and was subjected to observation by SEM.
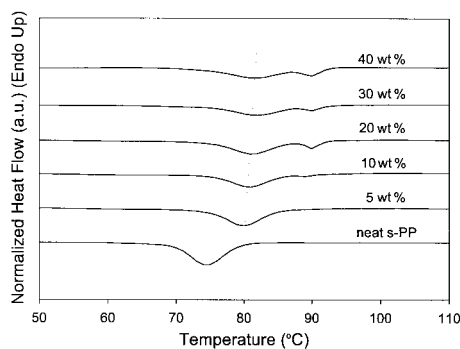
Figure 1 Non-isothermal crystallization exotherms for neat s-PP and 1.9 μm, uncoated $CaCO_3$-filled s-PP samples at various filler contents (recorded at a cooling rate of 10°C/min).

Shear viscosity measurements

The steady-state shear viscosity for both neat and $CaCO_3$-filled s-PP compounds was determined at 200°C in two different types of rheometers. An Instron 3213 capillary rheometer was used to study the steady-state shear behavior for both neat and $CaCO_3$-filled s-PP compounds at "high" shear rates (50 to 3,000 s^{-1}). The capillary was a tapered type having a 45° entrance angle. The barrel diameter was 9.525 mm. The number 1860 capillary die with a 1.25 mm diameter and a 50.19 mm length (L/D ratio = 40.15) was used in this study. An ARES Rheometric Scientific rheometer equipped with a parallel-plate fixture (8 mm diameter and 0.2 mm gap width) was used to study the steady-state shear behavior of these samples at "low" shear rates (0.25 to 25 rad/s).

RESULTS AND DISCUSSION

Non-isothermal crystallization and melting behavior

Figure 1 shows non-isothermal crystallization exotherms for neat and 1.9 μm uncoated $CaCO_3$-filled s-PP samples at various filler contents (recorded at a cooling rate of 10°C/min). Apparently, the crystallization (peak) temperature (T_{cl}) for the neat s-PP sample was observed at about 75°C. The incorporation of $CaCO_3$ particles shifted the T_{cl} value toward a higher temperature, but, upon further increase in the $CaCO_3$ content, the T_{cl} value only increased slightly. Figure 1 shows two types of crystallization exotherm. The first is the single-peak type (the peak temperature of which denotes T_{cl}), which was found for neat s-PP and s-PP samples loaded with "low" contents of 1.9 μm-uncoated $CaCO_3$ particles (approx. 0–10 wt %), and the second is the double-peak type (the peak temperature of the low-temperature peak denotes T_{cl}, while that of the high-temperature peak denotes T_{ch}), which was only found for s-PP samples loaded with "high" con-

tents of 1.9 μm uncoated $CaCO_3$ particles (approx. 20–40 wt %). Interestingly, s-PP samples loaded with $CaCO_3$ of larger particle sizes (2.8 and 10.5 μm) only exhibited a single-peak crystallization exotherm, regardless of the $CaCO_3$ content.

In order to verify whether the occurrence of the double crystallization exotherms on s-PP samples loaded with "high" contents of 1.9 μm-uncoated $CaCO_3$ particles (approx. 20–40 wt %) was an artifact or not, two separate experiments were carried out. The first involved assessing the effect of repeated heating and cooling, while the second investigated the effect of melt-annealing time on the crystallization behavior of s-PP samples filled with 40 wt % 1.9 μm-uncoated $CaCO_3$ particles. It should be noted that, in the first experiment, the melt-annealing time was 5 min, while in the second experiment the melt-annealing time varied from 5 to 30 min. The fusion temperature and cooling rate used in both experiments were fixed at 190°C and 10°C/min, respectively. According to Figure 2(a), it is clear that repeated heating and cooling affected neither the position nor the relative peak area of the two exotherms. In Figure 2(b), the effect of varying melt-annealing time on crystallization behavior of 40 wt % 1.9 μm uncoated $CaCO_3$-filled s-PP samples is illustrated. Clearly, variation in the melt-annealing time did not affect the position of the two
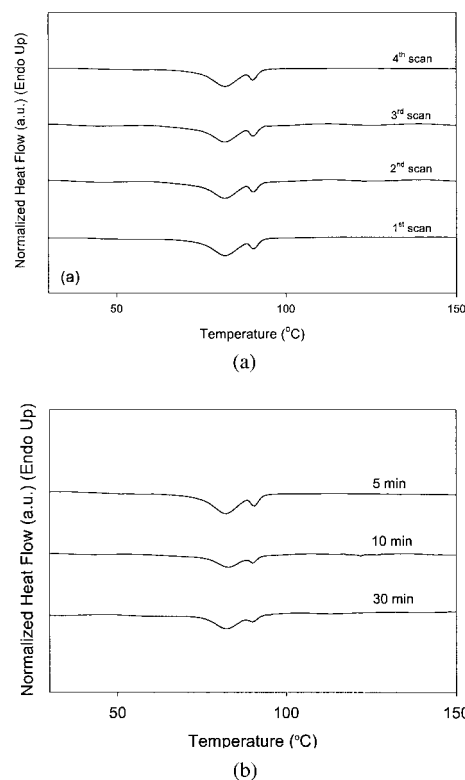

Figure 2 Effects of (a) repeated heating and cooling and (b) melt-annealing time on crystallization behavior of s-PP samples filled with 40 wt % 1.9 μm, uncoated $CaCO_3$ particles.

exotherms. However, it did affect their breadth and height. Since many samples were used to obtain this set of data, it is apparent that the double crystallization behavior observed was not an artifact and that the results are highly reproducible.

To a first approximation, the occurrence of double crystallization behavior for s-PP samples loaded with high contents of 1.9 μm uncoated $CaCO_3$ particles may be a result of the self-nucleation effect, likely attributable to the residual s-PP crystallites entrapped along the rough surface of $CaCO_3$ particles. In particular, the fact that the high-temperature crystallization peak occurred only in samples loaded with small $CaCO_3$ particles is most likely due to the high surface-area-to-volume ratio that these small particles exhibit, which could provide more rough sites on which s-PP crystallites become entrapped (in comparison with larger particles). Due to this entrapment, some of these crystallites may survive through the melting process, and, during subsequent cooling, they can act as predetermined nuclei to initiate crystallization.

If the above explanation is correct, it can be hypothesized that prolonged melting of s-PP samples loaded with high contents of 1.9 μm uncoated $CaCO_3$ particles should reduce the amount of residual s-PP crystallites entrapped along the rough surface of the particles. Furthermore, the entrapment of s-PP crystallites on the rough surface of the particles should be minimized when the $CaCO_3$ surface is coated with a non-nucleating substance (hence reducing the probability for these entrapped crystallites to self-nucleate the s-PP melt during subsequent cooling). Regarding the former hypothesis, the results shown in Figure 2(b) indicate that prolonged melting of 40 wt % 1.9 μm uncoated $CaCO_3$-filled s-PP samples at 30 min clearly reduced the intensity of the high-temperature crystallization exotherm. Regarding the latter, the crystallization exotherms recorded for samples loaded with 40 wt % 1.9 μm $CaCO_3$ particles with various types of surface treatment (stearic acid coated and paraffin-coated) exhibited only a single crystallization exotherm (results not shown). These observations suggest that the above explanation of the occurrence of the double crystallization behavior of s-PP samples loaded with high contents of 1.9 μm uncoated $CaCO_3$ particles are reasonable.

It should be noted at this point that the occurrence of double crystallization behavior was also reported for i-PP samples filled with 25 vol % 1.3 μm uncoated $CaCO_3$ (with the reported surface area of 5 m^2/g) by Pukánszky and Fekete.[14] They attributed the occurrence of double crystallization behavior to aggregation. They also observed that this phenomenon depends very much on the specific surface area of the filler and on the composition, and that it only appears on samples with fillers of high surface area. We do believe that aggregation did occur to a greater extent
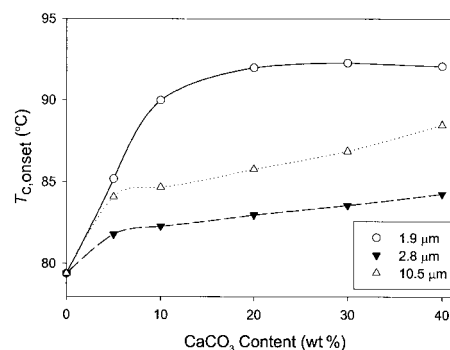

Figure 3 Crystallization (onset) temperature for neat s-PP and s-PP samples loaded with uncoated $CaCO_3$ particles of various sizes as a function of $CaCO_3$ content.

on $CaCO_3$ of smaller particle size, but it is less likely that aggregation itself can be attributed to the occurrence of double crystallization behavior observed in both s-PP and i-PP systems (or any other system). Apart from the self-nucleation effect of entrapped crystallites, which is thought to be the most likely explanation for double crystallization behavior, other possible explanations should not be ruled out entirely. These include multiple crystal modifications and the differences in crystallization behavior of the polymer on different parts of the particle surface (i.e. different parts have different nucleating efficiency).

The crystallization (onset) temperature $T_{c,\mathrm{onset}}$ values for neat s-PP and s-PP samples loaded with uncoated $CaCO_3$ particles of various sizes as a function of $CaCO_3$ content are reported in Figure 3, while Table II summarizes the non-isothermal crystallization results observed. According to Figure 3, it is apparent that the $T_{c,\mathrm{onset}}$ value increased with increasing $CaCO_3$ content, and, between samples loaded with 1.9 and 2.8 μm uncoated $CaCO_3$ particles, the $T_{c,\mathrm{onset}}$ value was found to increase with decreasing particle size (for a given filler loading). Interestingly, for samples loaded with 10.5 μm uncoated $CaCO_3$ grade, the $T_{c,\mathrm{onset}}$ value was found to lie between those of samples loaded with 1.9 and 2.8 μm uncoated $CaCO_3$ particles, instead of falling below them as expected. It has been mentioned previously that the as-received 10.5 μm uncoated $CaCO_3$ grade contained not only calcite but dolomite as well. The enhancement of the nucleating efficiency of $CaCO_3$ must be due to the presence of dolomite and the reason for this enhancement is not yet certain, since calcite and dolomite were found to have a similar unit cell (a trigonal unit cell) and very similar unit cell parameters.[15,16] A possible explanation may rely on the relative characteristics of the surface free energy between calcite and s-PP crystallites and dolomite and s-PP crystallites.

According to Table II, the $T_{c,\mathrm{onset}}$ values obtained for 1.9 μm stearic acid-coated and 1.9 μm paraffin-coated $CaCO_3$-filled samples were lower than the value for

TABLE II
Characteristics of Non-Isothermal Crystallization Observed
for all of the Samples Studied

Material	Content (wt %)	Crystallization Characteristics			
		$T_{c,onset}$ (°C)	T_{cl} (°C)	T_{ch} (°C)	ΔH_c (J/g)
Neat s-PP	0	79.4	74.4	-	33.5
1.9 μm-Uncoated s-PP	5	85.2	79.9	-	33.5
	10	90.0	80.8	-	34.8
	20	92.0	81.2	89.8	32.0
	30	92.3	81.9	89.9	24.4
	40	92.1	81.5	90.5	19.1
2.8 μm-Uncoated s-PP	5	81.8	76.8	-	28.4
	10	82.3	77.6	-	26.6
	20	83.0	78.2	-	16.8
	30	83.6	79.0	-	17.6
	40	84.3	79.4	-	10.1
10.5 μm-Uncoated s-PP	5	84.1	79.1	-	30.5
	10	84.7	79.6	-	27.1
	20	85.8	80.5	-	29.1
	30	86.9	81.3	-	22.3
	40	88.5	81.9	-	21.9
1.9 μm-Stearic acid-coated s-PP	5	81.7	76.7	-	28.6
	10	82.4	77.3	-	29.7
	20	83.2	78.3	-	24.2
	30	84.4	79.1	-	28.4
	40	84.8	79.5	-	23.8
1.9 μm-Paraffin-coated s-PP	5	81.4	76.2	-	29.1
	10	81.7	76.7	-	28.8
	20	81.9	77.3	-	28.4
	30	82.7	77.8	-	24.6
	40	83.2	78.4	-	19.8

1.9 μm uncoated $CaCO_3$-filled samples at the same filler loading. Clearly, the nucleating efficiency of $CaCO_3$ was reduced by such surface treatments. This is in a good agreement with results obtained by Rybnikar,[17] in which he reports that the nucleating efficiency of $CaCO_3$ could be increased or decreased by a suitable surface treatment. He also found that stearic acid coating on $CaCO_3$ has an adverse effect on the nucleating efficiency of $CaCO_3$ in i-PP. Referring to the aforementioned findings, the coating of $CaCO_3$ surface reduces the tendency for s-PP molecules to be partially absorbed, thus reducing the total amount of entrapped s-PP crystallites, which decreases in the probability of their initiating crystallization. At this point, it is worthy to note that nucleating efficiency of $CaCO_3$ depends very much on its purity, surface properties (i.e. specific surface area and type of surface modification), and average particle size.

Crystallization studies are incomplete without information about subsequent melting behavior. Figure 4 shows the subsequent melting endotherms for neat and 1.9 μm uncoated $CaCO_3$-filled s-PP samples at various filler contents (recorded at a heating rate of 20°C/min). Under the crystallization conditions studied, some samples with single crystallization peaks showed double melting endotherms in their heating scans, while others with double crystallization peaks showed three melting endotherms. The occurrence of double melting endotherms in s-PP is fully explained in an earlier report,[18] in which the low-temperature melting endotherm (the peak temperature of which denotes T_{ml}) corresponds to the melting of primary crystallites formed (at T_{cl}), and the high-temperature melting peak (the peak temperature of which denotes T_{mh}) corresponds to the melting of re-crystallized crystallites formed during a heating scan.
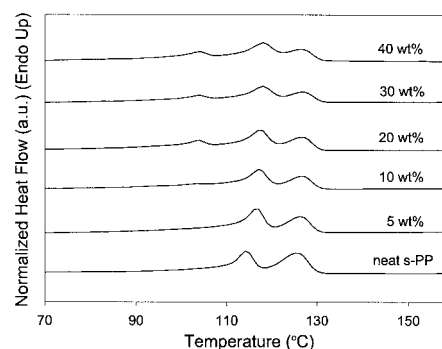

Figure 4 Subsequent melting endotherms for neat s-PP and 1.9 μm, uncoated $CaCO_3$-filled s-PP samples at various filler contents (recorded at a heating rate of 20°C/min).

TABLE III
Characteristics of Subsequent Melting Observed for All Samples Studied Including WAXD Degree of Crystallinity

Material	Content (wt %)	Melting characteristics					
		$T_{m,\text{onset}}$ (°C)	T_{ml2} (°C)	T_{ml} (°C)	T_{mn} (°C)	ΔH_m (J/g)	χ^{WAXD} (%)
Neat s-PP	0	110.0	-	114.4	125.5	33.8	16.2
	5	112.0	-	116.7	126.4	34.0	13.7
	10	112.2	-	117.2	126.9	33.6	-
1.9 μm-Uncoated s-PP	20	112.1	103.7	117.5	126.9	31.4	12.5
	30	112.0	104.0	118.0	127.1	25.9	-
	40	111.5	104.1	118.0	127.0	22.0	9.7
	5	111.0	-	115.4	125.9	33.5	13.1
	10	111.2	-	115.5	125.8	32.1	-
2.8 μm-Uncoated s-PP	20	111.5	-	116.1	126.3	33.8	11.4
	30	111.5	-	116.0	126.0	28.7	-
	40	111.4	-	116.1	126.0	26.8	9.8
	5	112.2	-	116.7	126.8	36.2	13.4
	10	112.1	-	116.7	126.6	32.9	-
10.5 μm-Uncoated s-PP	20	112.2	-	117.0	126.6	28.5	13.0
	30	111.9	-	117.4	126.6	27.9	-
	40	111.6	-	117.5	126.4	23.9	9.6
	5	111.0	-	115.5	126.0	33.4	11.7
	10	111.3	-	115.8	126.1	32.7	-
1.9 μm-Stearic acid-coated s-PP	20	111.7	-	115.8	125.6	27.6	11.3
	30	112.1	-	116.1	126.3	23.0	-
	40	112.1	-	116.4	126.3	19.7	9.9
	5	110.5	-	114.8	125.6	31.2	14.2
	10	110.9	-	115.1	125.6	30.2	-
1.9 μm-Paraffin-coated s-PP	20	111.1	-	115.5	125.8	29.9	13.0
	30	111.2	-	115.6	125.8	26.3	-
	40	111.4	-	115.7	125.8	22.1	12.4

According to Figure 4, another low-temperature melt endotherm (the peak temperature of which denotes T_{ml2}) observed on subsequent melt endotherms of s-PP loaded with high contents of 1.9 μm uncoated $CaCO_3$ particles (approx. 20–40 wt %) must correspond to the high-temperature crystallization peak observed on crystallization exotherms (see Fig. 1). This is rather surprising since the comparatively low value of T_{ml2} suggests low stability of the crystallites, despite their being formed at relatively high temperatures (T_{ch}). The reason for this unexpected behavior is not certain at this point. When considering the resulting T_{ml} values for s-PP samples loaded with uncoated $CaCO_3$ particles of various sizes as a function of $CaCO_3$ content (not shown), it is evident that the results obtained agreed particularly well with the crystallization results (see Fig. 3) in that the T_{ml} value increased with increasing $CaCO_3$ content. Also, between samples loaded with 1.9 and 2.8 μm uncoated $CaCO_3$ particles, the T_{ml} value was found to increase with decreasing particle size, and that of the samples loaded with 10.5 μm uncoated $CaCO_3$ fell essentially in between. Table III summarizes the results regarding subsequent melting behavior obtained for all of the samples studied.

Crystal structure and crystallinity

In order to observe the crystal structure and the resulting apparent degree of crystallinity of the various s-PP/$CaCO_3$ compounds investigated, a WAXD technique was utilized. Figure 5(a) shows the WAXD patterns for neat and 1.9 μm uncoated $CaCO_3$-filled s-PP samples at various filler contents. Each sample was prepared in the DSC cell at a cooling rate of 10°C/min. For the neat s-PP sample, the characteristic X-ray peaks were observed at the scattering angles 2θ of about 12.2, 15.9, 20.6 and 24.6°, corresponding to the limit-disordered form I[19–21] (according to the most recent nomenclature suggested by De Rosa et al.[22]), which has an orthorhombic unit cell with axes a = 14.5 Å, b = 5.6 Å, and c = 7.4 Å. According to this unit cell, the characteristic X-ray peaks should be observed at angles 2θ of about 12.2, 15.8, 20.8 and 24.5°, corresponding respectively to the reflection planes of (200), (010), (111), and (400). Comparison to isothermally crystallized neat s-PP samples reported earlier[23] suggests that the reflection onto (010) planes for non-isothermally crystallized neat s-PP samples (in this study) was much less pronounced.

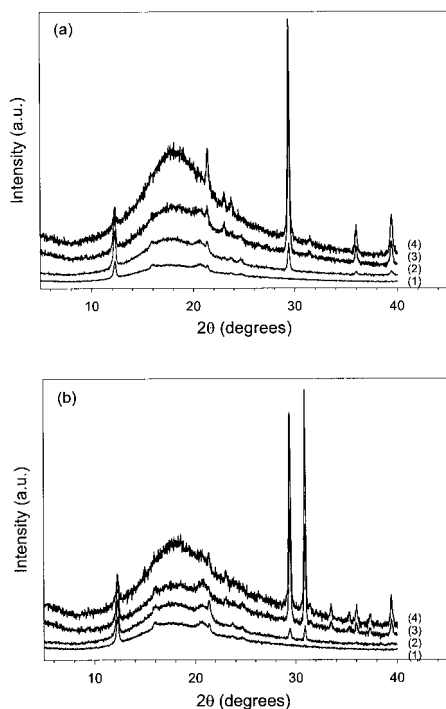In Figure 5(a), the effect of $CaCO_3$ content on the diffractograms of neat s-PP and s-PP samples filled

Figure 5 WAXD patterns for (a) neat s-PP and 1.9 μm, uncoated CaCO$_3$-filled s-PP samples and (b) neat s-PP and 10.5 μm, uncoated CaCO$_3$-filled s-PP samples at various filler contents: (1) 0 wt %, (2) 5 wt %, (3) 20 wt %, and (4) 40 wt %.

with 1.9 μm uncoated CaCO$_3$ particles is obvious. As CaCO$_3$ content increases, the intensities of the characteristic X-ray peaks of s-PP crystallites becomes less pronounced, with the characteristic peaks at an angle 2θ of about 15.9° disappearing when CaCO$_3$ content is greater than about 5 wt % and those at angles 2θ of about 20.6 and 24.6° disappearing altogether when CaCO$_3$ content is greater than about 20 wt %. On the other hand, the major characteristic peaks of calcite at angles 2θ of about 29.0 and 39.4° are evident when CaCO$_3$ content is greater than 5 wt % and become more pronounced and intensified with increasing CaCO$_3$ content. With the exception of s-PP samples loaded with 10.5 μm uncoated CaCO$_3$ particles, similar behavior is observed for s-PP samples filled with 2.8 μm uncoated CaCO$_3$ particles.

Figure 5(b) shows the WAXD diffractograms of neat s-PP and s-PP samples filled with 10.5 μm uncoated CaCO$_3$ particles. It is clear that, with increasing CaCO$_3$ content, the intensities of the characteristic X-ray peaks of s-PP crystallites become less pronounced, with the characteristic peaks at angles 2θ of about 15.9, 20.6 and 24.6° disappearing altogether when CaCO$_3$ content is greater than about 20 wt %. Similarly, major characteristic peaks of calcite at angles 2θ of about 29.0 and 39.4° were apparent when CaCO$_3$ content was greater than 5 wt % and became more pronounced and intensified with increasing CaCO$_3$ content. An

additional characteristic X-ray peak at an angle 2θ of about 30.9°, which is attributed to dolomite, is also evident when CaCO$_3$ content is greater than 5 wt % and becomes more pronounced and intensified with increasing CaCO$_3$ content.

The results shown in Figures 5(a, b) suggest that the presence of CaCO$_3$ particles does not alter the crystal structure of the crystallizing s-PP in the matrix. It does, however, affect the apparent degree of crystallinity, χ^{WAXD}, of the s-PP matrix. By referring to the relative ratio of the integrated intensities under the crystalline peaks A_c to the integrated total intensity A_t ($A_t = A_c + A_a$, where A_a is the integrated intensity under the amorphous halo), the following equation can be derived:

$$\chi^{\text{WAXD}} = \frac{A_c}{A_c + A_a} \in [0,1], \tag{1}$$

It is qualitatively obvious that the WAXD degree of crystallinity χ^{WAXD} decreases with increasing CaCO$_3$ content. It should be noted that contributions from the crystalline peaks of calcite and dolomite were excluded from the calculation. The observed χ^{WAXD} values for all of the samples studied are summarized in Table III.

Mechanical properties

Tensile properties

According to Figure 6(a), the tensile strength values for neat s-PP and s-PP samples filled with uncoated CaCO$_3$ particles of various sizes were found to decrease gradually with increasing CaCO$_3$ content (approx. 18.5–13 MPa), with the exception of samples filled with very low contents of 1.9 μm uncoated CaCO$_3$ (less than ≈5 wt %) which seem to increase to a maximum and then decrease. The decrease of tensile strength is probably due to the poor interfacial adhesion between the CaCO$_3$ surface and the s-PP matrix, resulting in poor stress transfer across the interface. The fact that the results were not affected by variation in the particle size suggests that the tensile strength is controlled primarily by the filler content rather than by its size. When compared to the results obtained for samples loaded with 1.9 μm uncoated CaCO$_3$ particles, both stearic acid and paraffin coating on the CaCO$_3$ particles resulted in the reduction of the tensile strength of the s-PP/CaCO$_3$ compounds [see Fig. 6(b)]. On the other hand, the Young's modulus was found to increase with increasing CaCO$_3$ content (approx. 440–700 MPa), as shown in Figure 7(a). This may be due to the stiffening effect, a direct result of the presence of the rigid dispersed phase of CaCO$_3$ particles within the s-PP matrix, and the increase in the number of crystallites nucleated by CaCO$_3$. As compared to the results obtained for samples loaded with 1.9 μm uncoated CaCO$_3$ particles, both stearic acid and paraffin
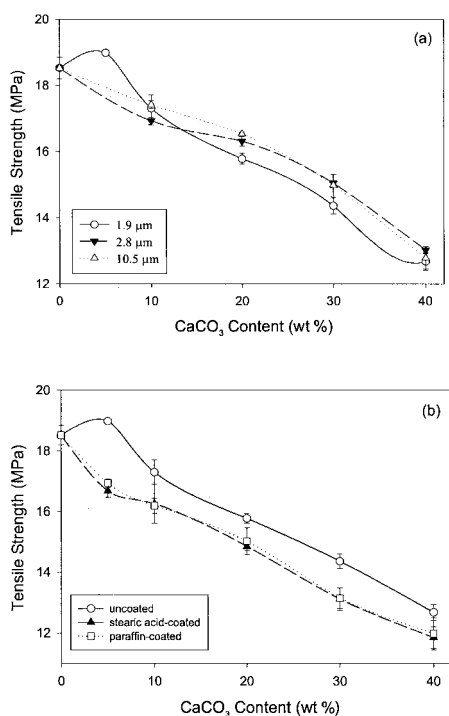
Figure 6 Tensile strength of neat s-PP and s-PP/CaCO₃ compounds as a function of CaCO₃ content exhibiting (a) the effect of varying particle size and (b) the effect of surface coating.

coating on the CaCO₃ particles resulted in the reduction of the Young's modulus [see Fig. 7(b)].

The influence of glass beads and talcum on the mechanical properties of s-PP was reported by Stricker et al.[11] The s-PP resins used in their work had the following molecular characteristics: for SPH-4 resin, M_n = 106,000 Da, M_w/M_n = 1.7, (%rr) = 82.2%; and, for SPH-40 resin, M_n = 80,000 Da, M_w/M_n = 1.7, and (%rr) = 91.1%. The glass beads had an average diameter of 5 μm and were coated with 0.02 wt % aminopropyltrimethoxysilane, and the talcum had an average diameter of 10 μm. They found that the Young's moduli of both functionalized glass bead-filled and talcum-filled s-PP increased with increasing filler volume content (0–30 vol %), with those for glass bead-filled samples (for both resins) increasing from about 375 to 800 MPa and those for talcum-filled samples (for SPH-4 resin) increasing from about 370 to 1,250 MPa (see Fig. 1 in ref. 11). When simultaneously comparing filler loading (at approx. 18 vol % or 40 wt % for CaCO₃-filled s-PP), the Young's modulus of CaCO₃-filled s-PP (approx. 700 MPa) was found to be greater than that of glass bead-filled s-PP (approx. 620 MPa), while it was lower than that of talcum-filled s-PP (approx. 900 MPa).

Impact resistance

The Izod impact resistance of neat s-PP and s-PP samples filled with uncoated CaCO₃ particles of various

sizes was, in general, found to decrease with increasing particle size and CaCO₃ content [see Fig. 8(a)]. Interestingly, the samples filled with low contents of 1.9 μm uncoated CaCO₃ particles (< approx. 10 wt %) showed a maximum Izod impact resistance value. The increase in the impact resistance at low filler contents may be attributed to the formation of smaller crystallites, as well as to the ability to absorb more energy by the increased portion of the amorphous phase.[24] The main reason for the decrease in impact resistance of s-PP/CaCO₃ compounds with increasing CaCO₃ content is likely the poor adhesion at the s-PP/CaCO₃ interface. Upon failure, cracks tend to preferentially propagate along the weaker interfacial region rather than through the polymer matrix, because of the higher resistance to propagation within the polymer matrix.[25]

The effect of surface modification of 1.9 μm CaCO₃ particles on the Izod impact resistance of filled s-PP samples is shown in Figure 8(b). Generally, the impact resistance of samples filled with surface-modified CaCO₃ particles was better than that of samples filled with unmodified CaCO₃. Interestingly, samples loaded with paraffin-coated CaCO₃ particles exhibited much greater impact resistance than those with uncoated and stearic acid-coated CaCO₃ ones. Riley et al.[26] reported that, for i-PP/CaCO₃ compounds, surface coating on CaCO₃ particles with stearic acid
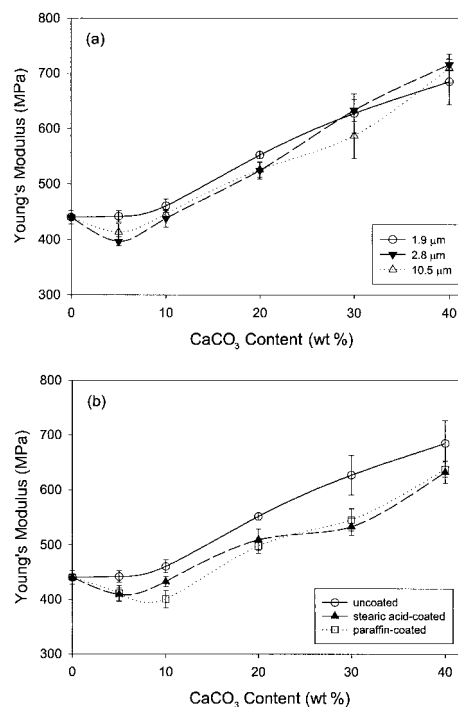

Figure 7 Young's modulus of neat s-PP and s-PP/CaCO₃ compounds as a function of CaCO₃ content exhibiting (a) the effect of varying particle size and (b) the effect of surface coating.
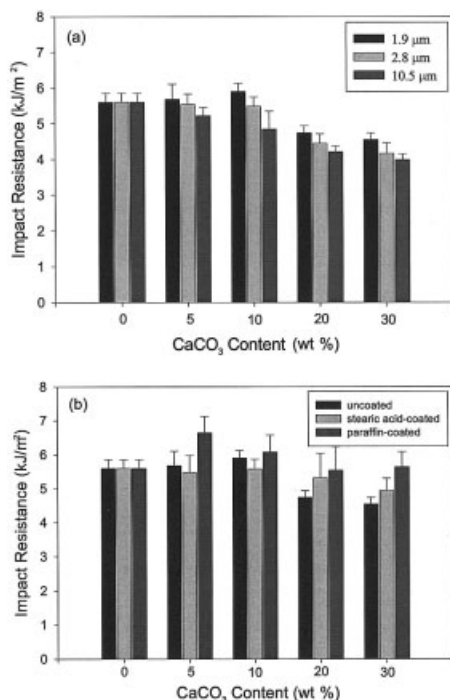
Figure 8 Izod impact resistance of neat s-PP and s-PP/CaCO$_3$ compounds as a function of CaCO$_3$ content exhibiting (a) the effect of varying particle size and (b) the effect of surface coating.

helped the dispersion of CaCO$_3$ particles in the i-PP matrix. Better dispersion means a larger number of discrete filler particles to help retard crack propagation (viz. a larger effective area along the s-PP/CaCO$_3$ interface to help absorb the impact energy).

Morphology of fracture surface

In order to verify the poor interfacial adhesion at the s-PP/CaCO$_3$ interface and determine whether stearic acid and paraffin coating of CaCO$_3$ particles really help its dispersion in the s-PP matrix, SEM was used to observe the fracture surfaces of selected fracture samples obtained from the impact testing.

SEM micrographs of the fractured surfaces of selected impact test specimens for s-PP filled with 20 wt % 1.9, 2.8, and 10.5 μm uncoated CaCO$_3$ particles are shown in Figures 9(a–c), respectively; while those for s-PP filled with 40 wt % 1.9, 2.8, and 10.5 μm uncoated CaCO$_3$ samples are shown in Figures 9(d–f), respectively. According to these micrographs, the dispersion of uncoated CaCO$_3$ particles appears to be rather uniform. However, for specimens loaded with 40 wt % 1.9 and 2.8 μm uncoated CaCO$_3$ particles [see Fig. 9(d, e)], large agglomerates are evident. This is mainly due to the fact that the small particles have large surface area, causing them to aggregate fairly easily, especially at high filler contents.[14] Careful examination of all mi-

crographs suggests that CaCO$_3$ particles are pulled out of the s-PP matrix rather easy (as evidenced by the smooth surface of the pull-out sites). This clearly indicates that the adhesion between CaCO$_3$ particles and the s-PP matrix is poor.

The effects of stearic acid and paraffin coating of CaCO$_3$ particles on their dispersion within the s-PP matrix were also investigated. Figures 9(a) and 10(a, b) respectively show SEM micrographs of the fractured surfaces of selected impact test specimens for s-PP filled with 20 wt % uncoated, stearic acid-coated and paraffin-coated 1.9 μm CaCO$_3$ particles. Figures 9(d) and 10(c,d) respectively show those for s-PP filled with 40 wt % uncoated, stearic acid-coated and paraffin-coated 1.9 μm CaCO$_3$ particles. For the CaCO$_3$ contents studied, CaCO$_3$ particles were well dispersed without appreciable agglomeration when their surfaces were coated with stearic acid and paraffin. It is also obvious from these micrographs that the adhesion between the coated CaCO$_3$ particles and the s-PP matrix was not improved, suggesting that surface modification of CaCO$_3$ particles with stearic acid and paraffin only helped the dispersion of the particles within the matrix.

Shear viscosity

The processability of s-PP/CaCO$_3$ compounds can be assessed by measuring their steady-state shear viscos-
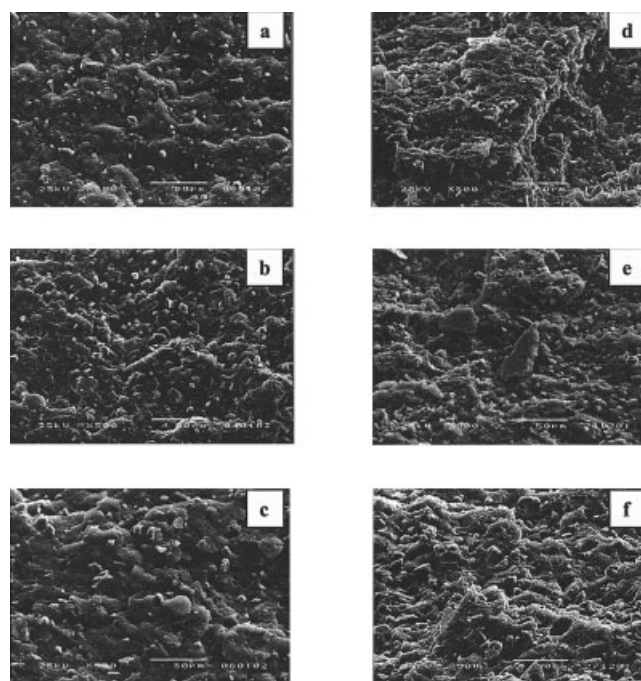

Figure 9 SEM micrographs of fractured surfaces of selected impact test specimens for s-PP filled with (a) 1.9, (b) 2.8, and (c) 10.5 μm, uncoated CaCO$_3$ particles at 20 wt % and (d) 1.9, (e) 2.8, and (f) 10.5 μm, uncoated CaCO$_3$ samples at 40 wt %.
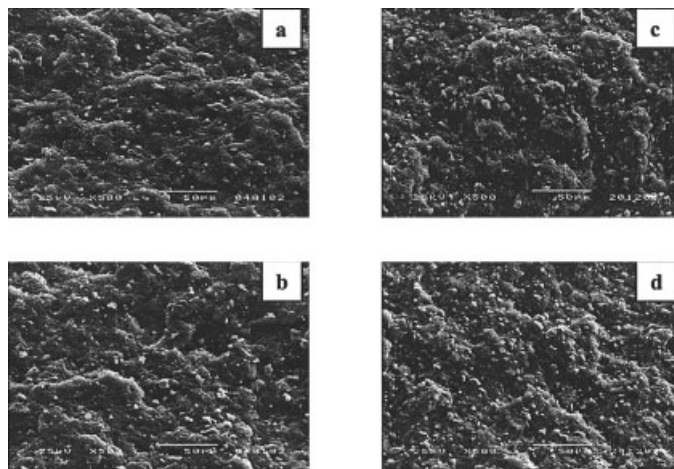
Figure 10 SEM micrographs of fractured surfaces of selected impact test specimens for s-PP filled with (a) stearic acid-coated and (b) paraffin-coated 1.9 μm CaCO$_3$ particles at 20 wt % and (c) stearic acid-coated and (d) paraffin-coated 1.9 μm CaCO$_3$ samples at 40 wt %.

ity. The steady-state shear viscosity of s-PP/CaCO$_3$ compounds was measured over a shear-rate range of 0.25 to 3,000 s^{-1} at a fixed temperature of 200°C. Two different types of rheometers were used: a parallel-plate rheometer (to cover a shear-rate range of 0.25 to 25 s^{-1} and a capillary rheometer (to cover a shear-rate range of 50 to 3,000 s^{-1}). The dependence of the steady-state shear viscosity of s-PP/CaCO$_3$ compounds on content, particle size, and type of surface modification of CaCO$_3$ particles was investigated.

The steady-state shear viscosity of neat and 1.9 μm uncoated CaCO$_3$-filled s-PP samples of various filler contents as a function of shear rate is shown in Figure 11. Apparently, the neat and 1.9 μm uncoated CaCO$_3$-filled s-PP samples of "low" filler loadings (approx. 5–20 wt %) exhibited typical shear thinning behavior, with a plateau region observed at low rates (< approx. 1 s^{-1}) and a shear thinning region at high shear rates (> approx. 1 s^{-1}). At high filler loadings (>

approx. 20 wt %), however, the compounds exhibited shear thinning behavior as well, but without the presence of a plateau region at low shear rates, and the viscosity values were always non-Newtonian and became increasingly nonlinear and unbounded with decreasing shear rate. Such an unbounded shear viscosity represents yielding as predicted by most viscoelastic models in which the apparent viscosity approaches infinity at vanishing shear rates, a direct result of the presence of yield stress below which there is no flow.[27,28] The other compounds filled with larger par-
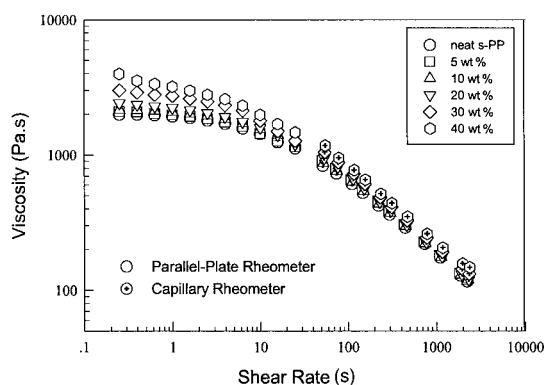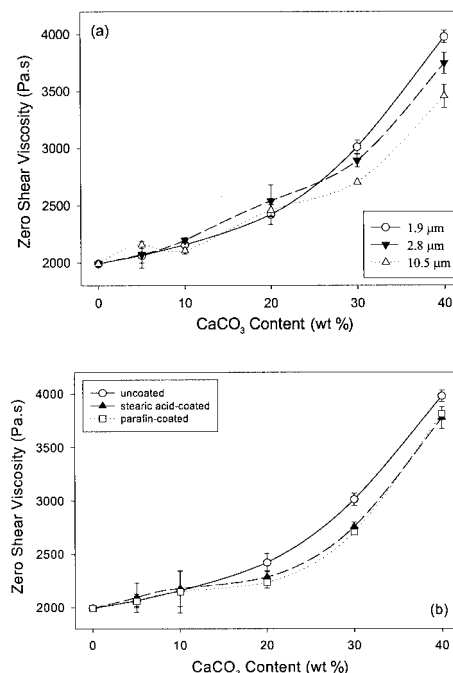

Figure 11 Steady-state shear viscosity of neat s-PP and 1.9 μm, uncoated CaCO$_3$-filled s-PP samples of various filler contents as a function of shear rate.

Figure 12 Zero shear viscosity of neat s-PP and s-PP/CaCO$_3$ compounds as a function of CaCO$_3$ content.

ticle sizes (2.8 and 10.5 μm) also exhibited similar behavior to that described above.

Figure 12(a) compares the zero shear viscosity values (taken as the viscosity values at a shear rate of approx. 0.25 s^{-1}) of neat s-PP and s-PP/CaCO$_3$ samples filled with CaCO$_3$ particles of various particle sizes as a function of CaCO$_3$ content. Apparently, the zero shear viscosity values were found to increase monotonically with increasing filler loading. It should be noted that the enhancement of the shear viscosity due to the presence of non-interactive rigid particles in dilute suspensions was proposed long ago by Einstein,[29,30] who pointed out that the enhancement of the shear viscosity is a result of increased energy dissipation due to the presence of the particles. In more concentrated systems, stronger interactions between filler particles give rise to much larger energy dissipation, resulting in much stronger viscosity enhancement.[31] This is exactly the reason for the profound increase in the zero shear viscosity values at high filler loadings observed for the s-PP/CaCO$_3$ compounds.

Another interesting observation from data shown in Figure 12(a) is that, among samples loaded with uncoated CaCO$_3$ at high filler loadings (> approx. 20 wt %), 1.9 μm uncoated CaCO$_3$-filled s-PP samples exhibited the highest zero shear viscosity value. It is a known fact that the smaller the filler particles, the larger the surface area, giving rise to a greater possibility of the formation of inter-particular structure. As a result of the strong inter-particular interactions, the enhancement of the shear viscosity for the samples filled with these fine CaCO$_3$ particles was apparent. However, when the surface of CaCO$_3$ particles was coated with stearic acid and paraffin, inter-particular interactions were affected in an adverse manner, as evidenced by the reduction in the zero shear viscosity values at high filler loadings (> approx. 10 wt %) [see Fig. 12(b)]. This is quite interesting, since SEM micrographs showed that the dispersion of CaCO$_3$ particles within the s-PP matrix was enhanced by such surface modifications. This implies that, even though it is responsible for improving particulate dispersion, surface modifications of CaCO$_3$ particles with stearic acid and paraffin reduce the inter-particular interactions as a result of the reduction of the effective area of the particles.

CONCLUSIONS

In this study, the effects of CaCO$_3$ with varying particle sizes (1.9, 2.8 and 10.5 μm), contents (0–40 wt %), and types of surface modification (uncoated, stearic acid-coated, and paraffin-coated) on crystallization and melting behavior, mechanical properties (tensile and impact properties), and processability (steady-state shear viscosity) of s-PP/CaCO$_3$ compounds were investigated.

Non-isothermal crystallization studies revealed that incorporation of CaCO$_3$ particles shifted the crystallization peak towards a higher temperature, but the increase in the crystallization peak only occurred very slightly with further increase in the CaCO$_3$ content. Two types of crystallization exotherm were observed: the single-peak type and the double-peak type. The double-peak type was only found for s-PP samples loaded with "high" contents of 1.9 μm uncoated CaCO$_3$ particles, which was postulated to be a result of the self-nucleation effect of residual s-PP crystallites entrapped along the rough surface of CaCO$_3$ particles. When considering the effect of CaCO$_3$ particle size on the crystallization behavior of s-PP/CaCO$_3$ compounds, it was found that the crystallization (onset) temperature increased with increasing CaCO$_3$ content and decreasing particle size. This general statement does not hold true, however, for samples loaded with 10.5 μm uncoated CaCO$_3$ particles, most likely due to the presence of dolomite. Surface coating of CaCO$_3$ particles with stearic acid and paraffin reduced the nucleating ability of the particles. WAXD results suggested that the incorporation of CaCO$_3$ did not affect the crystal structure of the crystallizing s-PP in the matrix, but it adversely affected the apparent degree of crystallinity.

In general, the tensile strength of s-PP/CaCO$_3$ compounds was found to decrease gradually with increasing CaCO$_3$ content, most likely due to the poor interfacial adhesion between the CaCO$_3$ surface and the s-PP matrix. The average size of CaCO$_3$ particles did not appear to affect the tensile strength noticeably. On the other hand, the Young's modulus was found to increase with increasing CaCO$_3$ content, most likely a result of the stiffening effect contributed by the presence of rigid particles. Both stearic acid and paraffin coating on the CaCO$_3$ particles resulted in the reduction of both the tensile strength and the Young's modulus. Similarly, the Izod impact resistance of samples loaded with uncoated CaCO$_3$ particles of various sizes was, in general, found to decrease with increasing particle size and content, most likely due to the poor interfacial adhesion between the s-PP/CaCO$_3$ interface. Both stearic acid and paraffin coating on the CaCO$_3$ particles helped to improve the Izod impact resistance, a result of the improved dispersion within the s-PP matrix.

Lastly, the inclusion of CaCO$_3$ particles to a large extent affected the shear viscosity of s-PP/CaCO$_3$ compounds. The zero shear viscosity was found to increase monotonically with increasing CaCO$_3$ content, with the samples loaded with 1.9 μm uncoated CaCO$_3$ particles exhibiting the highest value, possibly due to the formation of inter-particular structures of these small, rigid particles. The zero shear viscosity was reduced when the surface of CaCO$_3$ particles was

coated with either stearic acid or paraffin, most likely a result of the reduced inter-particular interactions.

References

1. Ewen, J. A.; Johns, R. L.; Razavi, A.; Ferrara, J. D. J Am Chem Soc 1988, 110, 6255.
2. Natta, G.; Pasquon, I.; Zambelli, A. J Am Chem Soc 1962, 84, 1488.
3. Rodriguez-Arnold, J.; Bu, Z.; Cheng, S. Z. D. J Macromol Sci-Rev Macromol Chem Phys 1995, C35, 117.
4. Schardl, J.; Sun, L.; Kimura, S.; Sugimoto, R. J Plastic Film Sheeting 1996, 12, 157.
5. Sun, L.; Shamshoum, E.; DeKunder, G. SPE-ANTEC Proc 1996, 1965.
6. Gownder, M. SPE-ANTEC Proc 1998, 1511.
7. Sura, R. K.; Desai, P.; Abhiraman, A. S. SPE-ANTEC Proc 1999, 1764.
8. Guadagno, L.; Naddeo, C.; D'Aniello, C.; Di Maio, L.; Vittoria, V.; Acierno, D. Macromol Symp 2002, 180, 23.
9. Supaphol, P.; Spruiell, J. E. J Appl Polym Sci 2000, 75, 44.
10. Supaphol, P. J Appl Polym Sci 2000, 78, 338.
11. Stricker, F.; Bruch, M.; Mülhaupt, R. Polymer 1997, 38, 5347.
12. Stricker, F.; Mülhaupt, R. Polym Eng Sci 1998, 38, 1463.
13. Stricker, F.; Maier, R.-D.; Bruch, M.; Thomann, R.; Mülhaupt, R. Polymer 1999, 40, 2077.
14. Pukánszky, B.; Fekete, E. Polym Compos 1998, 6, 313.
15. Graf, D. L. Am Mineral 1961, 46, 1283.
16. Miser, D. E.; Swinnea, J. S.; Steinfink, H. Am Mineral 1987, 72, 188.
17. Rybnikar, F. J Appl Polym Sci 1991, 42, 2727.
18. Supaphol, P. J Appl Polym Sci 2001, 82, 1083.
19. Lovinger, A. J.; Lotz, B.; Davis, D. D.; Padden, F.J. Macromolecules 1993, 26, 3494.
20. Auriemma, F.; De Rosa, C.; Corradini, P. Macromolecules 1993, 26, 5719.
21. De Rosa, C.; Auriemma, F.; Vinti, V. Macromolecules 1997, 30, 4137.
22. De Rosa, C.; Talarico, G.; Caporaso, L.; Auriemma, F.; Galimberti, M.; Fusco, O. Macromolecules 1998, 31, 9109.
23. Supaphol, P.; Spruiell, J. E.; Lin, J.-S. Polym Int 2000, 49, 1473.
24. Maiti, S. N.; Mahapatro, P. K. J Appl Polym Sci 1991, 42, 3101.
25. Tjong, S. C.; Li, R. K. Y.; Cheung, T. Polym Eng Sci 1997, 37, 166.
26. Riley, A. M.; Paynter, C. D.; McGenity, P.M.; Adams, J.M. Plast Rub Proc Appl 1990, 14, 85.
27. Kim, K. J.; White, J. L. Polym Eng Sci 1999, 39, 2189.
28. Wang, Y.; Yu, M.-J. Polym Comp 2000, 21, 1.
29. Einstein, A. Ann Phys 1906, 19, 289.
30. Einstein, A. Ann Phys 1911, 34, 591.
31. Li, L.; Masuda, T. Polym Eng Sci 1990, 30, 841.